Наносистеми, наноматеріали, нанотехнології
Nanosistemi, Nanomateriali, Nanotehnologii
2024, т. 22, № 2, сс. 335–351
https://doi.org/10.15407/nnn.22.02.335

PACS numbers: 07.07.Df, 65.80.-g, 68.37.Ps, 81.07.Gf, 81.16.Be, 84.32.Ff, 85.35.Be

Silicon 1*D* Structures for Resistive and Diode Temperature Sensors

Yaroslav Linevych[1], Viktoriia Koval[1], Mykhailo Dusheiko[1], Maryna Lakyda[2], Yurii Yasiievych[1], and Serhii Maliuta[1]

[1]*National Technical University of Ukraine*
'Ihor Sikorsky Kyiv Polytechnic Institute',
37, Beresteyskyi Ave.,
UA-03056 Kyiv, Ukraine
[2]*National University of Life and Environmental Sciences of Ukraine,*
19, Horikhuvatskyi Shliakh Str., Bldg. 1, Of. 12,
UA-03041 Kyiv, Ukraine

Resistive and diode temperature sensors based on silicon nanowires (SiNWs) are fabricated. Silicon nanowires are obtained by two-stage metal-assisted chemical etching (MACE) technique. The influence of SiNWs synthesis parameters on device characteristics is investigated. In particular, the influence of the duration of the first and second stages of MACE, the content of solutions based on $AgNO_3$ and H_2O_2, the presence of textured surface of silicon wafer before the MACE process, additional processing in an isotropic/anisotropic etchant after the MACE process on the characteristics of temperature sensors is determined. The electrical and thermosensitive parameters for obtained sensors are calculated, namely, resistance, rectifying coefficient, and coefficient of thermosensitivity. A significant influence of the MACE-process parameters on the lateral roughness and volume porosity of the thermosensitive surface is determined. As established, the following technological operations lead to an increase in resistance: a raise in the deposition time of silver nanoparticles and the use of additional post-chemical treatment, as well as a decrease in the etching time and a decrease in the amount of H_2O_2. The resistance of the array of silicon nanowires is in the range of 27.6–199.6 Ω. As established, the following process parameters improve the rectifying characteristics: increasing the content of hydrogen peroxide, the presence of preliminary texturing of silicon surface, as well as the use of additional post-chemical treatment in an acid etchant. The maximum rectifying coefficient of diode temperature sensors is of 2503. Significant impact of process parameters on the lateral roughness and bulk porosity of the thermosensitive surface is revealed. As found, the thermal sensitivities of both diode sensors and resistive ones are improved with the increase of MACE first-stage parameters and the decrease of MACE second-stage parameters, as well as in the presence of acid etching treatment. The maximum thermal sensitivity coefficient of thermistors based on silicon nanowires is of 2336 ppm/K, while, for thermodiodes, this coefficient is of 2.5 mV/K.

Синтезовано резистивні та діодні сенсори температури на основі кремнійових нанониток (КНН). Кремнійові нанонитки було одержано методом двостадійного металостимульованого хемічного щавлення (МСХЩ). Досліджено вплив параметрів синтези КНН на характеристики приладів. Зокрема, було встановлено вплив тривалости першого та другого етапів МСХЩ, вмісту розчинів на основі $AgNO_3$ й H_2O_2, наявности текстури на поверхні кремнійової пластини до процесу МСХЩ, додаткового оброблення в ізотропному/анізотропному щавнику після процесу МСХЩ на характеристики сенсорів температури. Було розраховано електричні та термочутливі параметри для одержаних сенсорів, зокрема опору: коефіцієнт випрямлення та коефіцієнт термочутливости. Визначено значний вплив технологічних параметрів синтези масиву КНН на латеральну шерсткість та об'ємну пористість термочутливої поверхні сенсорів температури. Встановлено, що до збільшення опору приводять наступні технологічні операції: зростання часу осадження наночастинок срібла та використання додаткового пост-хемічного оброблення, а також зменшення часу щавлення та зменшення кількости H_2O_2. Розрахований опір масиву кремнійових нанониток знаходився в межах 27,6–199,6 Ω. Встановлено, що наступні технологічні параметри поліпшують випростувальні характеристики: збільшення вмісту перекису Гідроґену, наявність попереднього текстурування поверхні кремнійової пластини, а також використання додаткового пост-хемічного оброблення у кислотному щавнику. Максимальний коефіцієнт випростування діодних сенсорів температури склав 2503. Встановлено, що термочутливість як діодних, так і резистивних сенсорів поліпшується зі збільшенням параметрів першого етапу МСХЩ та зменшенням параметрів другого етапу МСХЩ, а також за наявности додаткового хемічного оброблення кислотним щавником. Максимальний коефіцієнт термочутливости термісторів на основі кремнійових нанониток становив 2336 ppm/K, тоді як для термодіод цей коефіцієнт становив 2,5 мВ/К.

Key words: metal-assisted chemical etching, silicon nanowires, thermodiode, thermistor.

Ключові слова: металостимулюване хемічне щавлення, кремнійові нанонитки, термодіода, термістор.

(Received 5 July, 2023)

1. INTRODUCTION

Temperature is one of the most measured physical parameters, as many industrial areas require temperature control in manufacturing processes, as well as during operation, for storage and transportation of devices, equipment, raw materials, food or pharmaceutical products, *etc*. Additionally, temperature measurement is an essential component of electronic device protection systems, such as computers, mobile phones, and others, where high temperatures can lead to a breakdown. Specifically, embedded thermistors on a motherboard prevent overheating when the workload increases or a fan fails.

Furthermore, temperature sensors allow monitoring temperature of the entire computer or individual components and smoothly adjusting fan speed, reducing noise levels during downtime. Currently, temperature sensors such as thermistors and thermodiode are used. The principle of operation of a monocrystalline thermistor is that its resistance decreases with increasing temperature. This is because the number of free charge carriers in the semiconductor increases with temperature, reducing its resistance. The most commonly used materials for thermistors are Ge [1], Si [2], and graphene [3].

These devices have such advantages as sensitivity to small temperature changes, excellent repeatability and significantly low hysteresis [4]. The disadvantages of thermistors include non-linearity of their thermosensitive characteristics, aging, and some instability in their characteristics. In certain cases, they are not compatible with CMOS technology. The principle of operation of a thermodiode is based on the decrease in voltage across the p-n junction with increasing temperature at a fixed level of current according to an almost linear law. The most commonly used materials for thermodiodes are Si [5] and Ge [6]. Thermodiodes have such advantages as low cost and almost linear voltage–temperature dependence over a wide range (from 4.2 K to 888 K). Despite being widely used sensors, thermodiodes also have their drawbacks, including low sensitivity and self-heating.

The use of various types of nanostructures in sensors is highly relevant today. These nanostructures include nanofilms [7, 8], nanoparticles [9, 10], nanofibers [11, 12], nanocrystals [13, 14], nanowires [15, 16], nanorods [17, 18], and so on. One-dimensional (1*D*) structures, such as nanowires, with widths up to 100 nm and lengths exceeding their width, possess a high aspect ratio (ranging from 10 to 100), making those highly promising materials in sensing. The larger area of lateral surface of these nanostructures allows for an increased number of molecules to be absorbed on the sensor surface, enhancing its response. Another important advantage of silicon nanowires is the ability to create complex sensor systems with high-density arrangements, which is crucial in many branches of industry.

Currently, silicon nanowires (SiNWs) can be synthesized within one of two approaches: 'top–down' and 'bottom–up' [19]. In the top–down approach, clusters of monocrystalline silicon are removed, resulting in the formation of one-dimensional structures (nanowires or pores). Within this approach, such methods of SiNWs obtaining can be distinguished: metal-assisted chemical etching (MACE) [20, 21], reactive ion etching (RIE) [22], and plasma chemical etching [23]. In the bottom–up approach, silicon nanowires are grown by assembling individual silicon atoms using the following techniques: chemical vapour deposition (CVD) [19, 24], vapour–liquid–solid (VLS) growth [19, 25], solution–liquid–solid (SLS) growth [19], laser ablation (LA) [26], and thermal evaporation of powder [26]. A comparison of the two most common methods within the two approaches, VLS and MACE, has shown that nanowires obtained through the vapour–liquid–solid growth exhibit a high degree of ordering in their arrangement, but they have a relatively low surface density. The advantages of the metal-assisted chemical etching include its simplicity of implementation, low cost, and the ability to synthesize a dense array of nanostructures with a high aspect ratio.

The aim of this research is to investigate the application of silicon nanowires in resistive and diode-type temperature sensors. For this purpose, metal-assisted chemical etching was used, and the influence of process parameters on the characteristics of temperature sensors based on silicon nanowires was studied.

2. EXPERIMENTAL PART

Device Fabrication. Resistive and diode temperature sensors were fabricated in this research. The resistive sensors consist of a SiNWs and two front contacts (labelled as 1 and 2 in Fig. 1). The diode sensors consist of a *p*–*n* junction, one front contact (either 1 or 2 in Fig. 1) and one back contact (labelled as 3 in Fig. 1). The initial Si wafers were of *p*-type conductivity with resistivity of 1 and 10 Ω·cm, both textured and non-textured. To synthesize the experimental samples, the silicon substrates were cleaned using a three-stage cleaning process [27]. The texturing process was performed to obtain a more developed surface by making of pyramids. For this, a solution of 970 ml H_2O/30 g KOH/70 ml IPA was used at a temperature of 75°C for 15 min. The synthesis of silicon 1*D* structures was performed using metal-assisted chemical etching (MACE), described in our previous work [29]. In this study, additional etchants were applied after the MACE process in order to remove the damaged layer on the SiNWs. The acid etchant $HF/HNO_3/CH_3COOH$ (1:4:4) at room temperature for 10 min provided isotropic etching of the surface, while the alkaline etchant NaOH/IPA/H_2O (2:10:88) at a temperature of 90°C for 10 min ensured anisotropic etching.

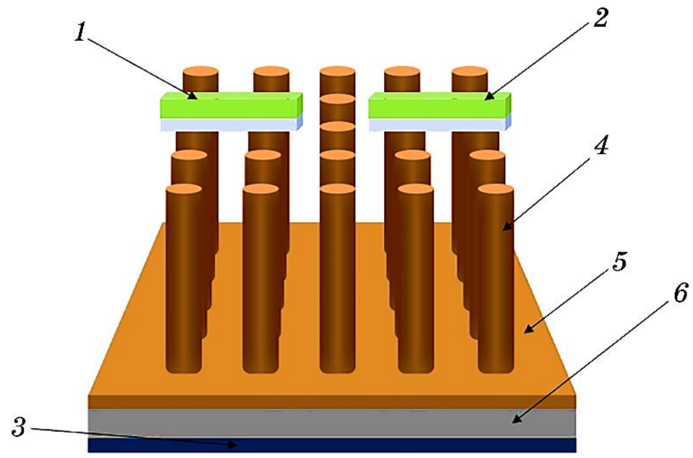

Fig. 1. Structure of a temperature sensor based on silicon nanowires: *1*, *2*—front contacts Ti–Ni; *3*—back contact Al; *4*—SiNWs; *5*—*n*-type Si; *6*—*p*-type Si.

Then, a *p*–*n* junction was obtained in the *p*-type SiNWs. Phosphorus was introduced into the SiNWs in a two-step process using a diffusion furnace: phosphorus predeposition (constant source diffusion) step at 750°C for 5 min and phosphorus drive-in at 830°C for 20 min. As a result, an *n*-type silicon layer with a sheet resistance of 50 Ω/□ was obtained. A continuous backside aluminium contact was deposited on the substrate using the DC magnetron sputtering. The operating parameters of the vacuum deposition system were as follows: voltage—400 V, current—4 A, argon pressure—$3\cdot10^{-4}$ mm Hg, deposition time—40 min. Subsequently, the aluminium film was annealed in a diffusion furnace at a temperature of 650°C in a nitrogen atmosphere. Thus, a backside contact with a thickness of 1.5 μm was obtained. For the formation of point front contacts (Ti/Ni), electron-beam deposition was used. The deposition parameters in the vacuum system were the following: chamber pressure—10^{-5} mmHg, voltage—13 kV, current—120 mA. The deposition time for titanium and nickel layers was 3 and 20 min, respectively. As a result, a front contact with thickness of approximately 0.5 μm was formed.

Characterization Techniques. To investigate the surface morphology of silicon substrates after MACE, an atomic force microscope (AFM) SolverPro was used in semi-contact mode. AFM images processing was performed using the Nova software with scanning areas of 50×50 μm, 20×20 μm, and 10×10 μm. The *I*–*V* characteristics of the obtained diode and resistive-type sensors were measured using the Power Supply HM8143 and the digital voltmeter MS8040. The quantitative evaluation of porosity of the silicon material was performed using the weight by means of OHAUS Pioneer PX163 analytical balances. The temperature characteristics of the experimental samples were measured in the range of 293 K to 353 K. Temperature stabilization in the thermal chamber was achieved using the digital temperature controller PULSE PT20-N2 with an accuracy of 1°C. The thermal sensitivity of the devices was evaluated in constant current mode for the diode and constant voltage mode for the resistor.

3. RESULTS AND DISCUSSION

Surface Morphology of Silicon Nanowires. Figure 2 shows the 2*D* and 3*D* views of the surface morphology of SiNWs array. In Figure 2, it can be observed that the array of SiNWs exhibits a high density. The structural parameters are presented in Table 1. The average height of silicon nanowires ranged from 1638 to 2328 nm, with a maximum height diapason from 3030 to 5440 nm. The porosity coefficient ranged from 56% to 96%.

It should be noted that the surface of the silicon wafer after MACE looks blurry and diffuse (Fig. 3, *a*). This can be attributed to the presence of a damaged surface layer and natural oxide. To remove these layers, both alkaline (anisotropic) and acidic (isotropic) etching were performed (Fig. 3, *c*, *d*). As shown in Figure 2, *b*, additional pre-texturing of the initial wafer leads to the formation of

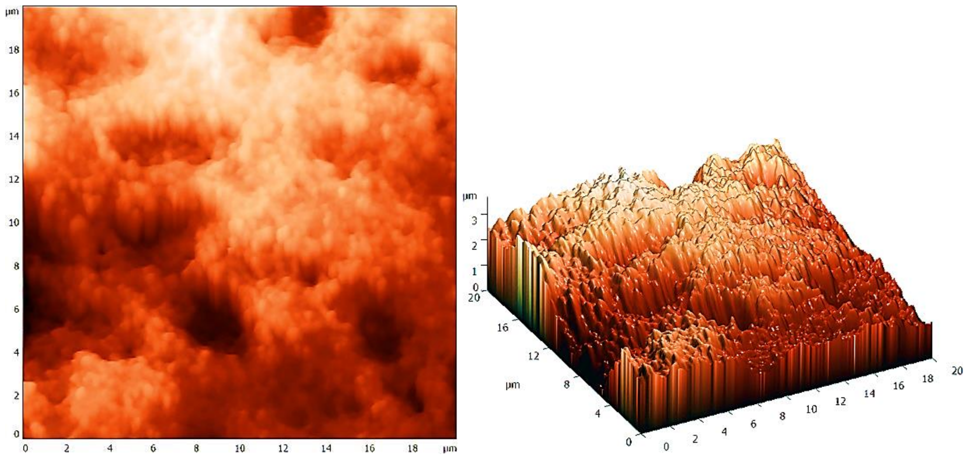

a *b*

Fig. 2. AFM images of SiNWs synthesized using the MACE technique: 2*D* view (*a*) and 3*D* view (*b*).

TABLE 1. MACE parameters of Si nanowire synthesis.

Sample number	Parameters of the standard MACE process				Additional chemical treatment before or after the MACE process	
	t_1, sec.	t_2, min	$AgNO_3$, mg	H_2O_2, ml	Texturing	Post-surface treatment
1	20	90	34	0,4	—	—
2	20	90	34	0,8	—	—
3	20	90	34	1,2	—	—
4	20	45	34	0,8	—	—
5	20	135	34	0,8	—	—
6	60	45	34	0,8	—	—
7	60	90	34	0,8	—	—
8	60	135	34	0,8	—	—
100	20	90	68	0.8	—	—
101	60	90	68	0.8	—	—
102	20	30	68	0.8	—	—
104	20	90	68	0.8	—	isotropic etching
105	20	90	68	0.8	+	anisotropic etching
106	20	90	68	0.8	+	—
109	60	30	68	0.8	+	—
110	20	90	68	0.8	+	isotropic etching
111	20	90	68	0.8	—	anisotropic etching
112	20	90	68	0.8	+	—
113	20	90	68	0.8	—	—

pyramid-like structures that randomly cover its surface and increase the surface roughness from 599 to 897 nm. However, a degree of porosity has decreased from 82.5% to 56%. This may be attributed to the fact that silver nanoparticles (Ag NPs) are deposited less effectively on the side surface of the pyramids. After undergoing treatment in an alkaline etchant, the width of the trenches between the SiNWs increases, and the surface becomes rougher. This is evidenced by the increase in surface roughness from 897 to 1006 nm. It can be due to the different etching rates, depending on the crystallographic orientations. As a result, predominantly lateral chemical etching of the trench-like pores is observed.

With the addition of an acidic etchant, isotropic etching takes place, which removes the rough surface layer of the material. This is indicated by the decrease in surface roughness from 897 to 771 nm. Additionally, a well-developed network of nanoscale pores is formed on the surface, which has a square shape with a side length of approximately 1 μm (Fig. 3, *d*) due to etching at an equal rate of

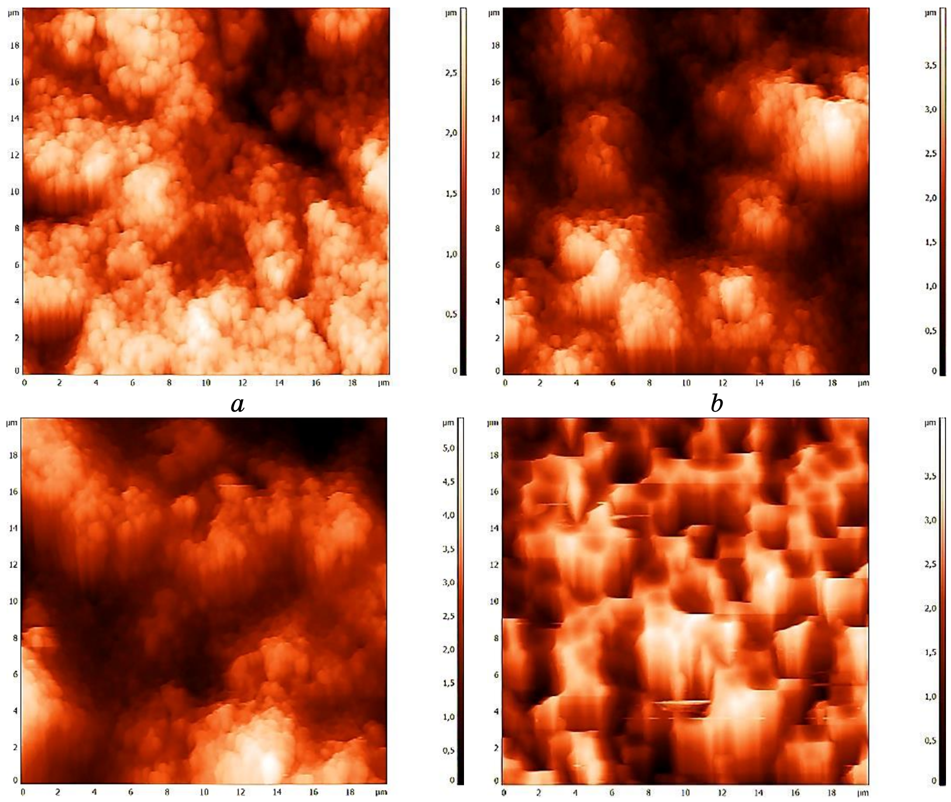

Fig. 3. AFM $2D$ images of SiNWs obtained using the MACE technique: without additional treatment (*a*), on a textured substrate (*b*), on a textured substrate with alkaline etching (*c*), on a textured substrate with acidic etching (*d*).

hills and pits. As can be seen in Fig. 3, the depth of the pores is determined by different shades: lighter shades indicate small pores, and darker shades indicate deeper pores. Such surface morphology of SiNWs will influence the characteristics of devices based on them. After the post-surface treatment, the degree of porosity of the initial textured surface increased from 56% to 92% (for isotropic etching) and to 96% (for anisotropic etching).

Resistive Temperature Sensors. The principle of operation of resistive temperature sensors involves a change in device resistance with temperature variation. The electrical and thermosensitive properties of these sensors were studied based on the volt-ampere characteristics (I–V) shown in Fig. 4, *a* and calculated coefficients of thermosensitivity (Table 2).

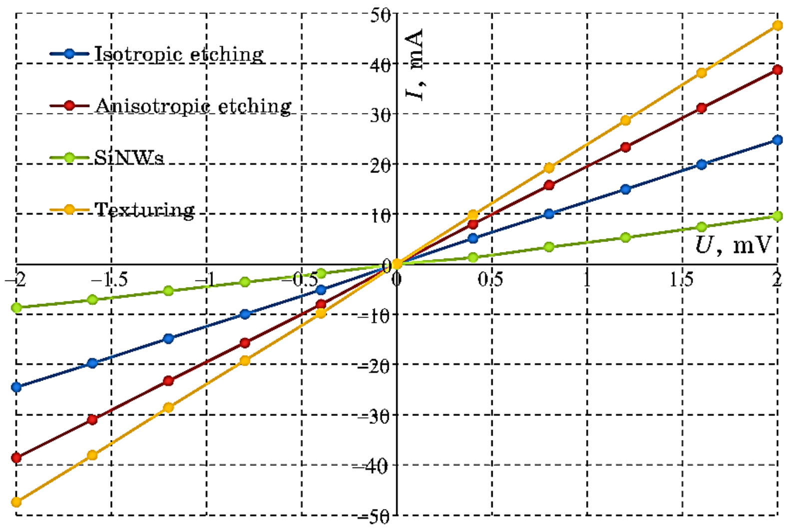

a

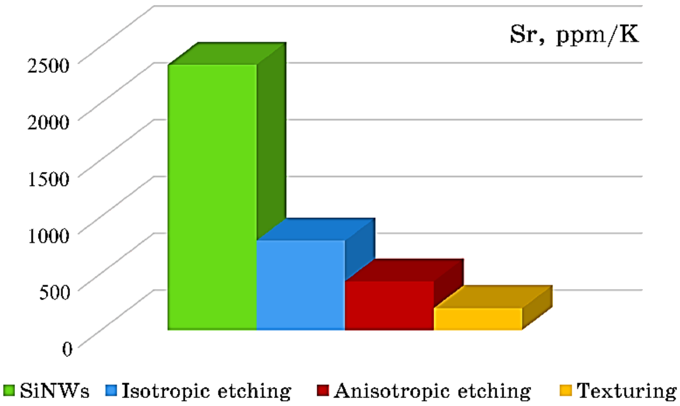

b

Fig. 4. *I*–*V* characteristics of thermistor based on SiNWs (*a*) and their thermosensitivity in dependence on additional-chemical treatment (*b*).

Produced resistive structures based on SiNWs are characterized by linear and symmetric *I*–*V* characteristics. Calculated resistance of the silicon nanowire array ranged from 27.6 to 199.6 Ω depending on the synthesis parameters: the change in resistance increased deposition time of Ag NPs and additional post-chemical treatment. For example, increasing deposition time of silver nanoparticles from 20 to 60 sec leads to an increase in sensor resistance from 27.6 to 91.8 Ω. This is probably due to the formation of a well-developed surface, as evidenced by the increase in r.m.s. from 226 to 753 nm and the increase in porosity from 82.5% to 98%. The use of an

TABLE 2. Influence of texturing and post-chemical treatment on surface morphology for SiNWs.

Parameters of surface morphology	SiNWs	SiNWs/acidic etching	SiNWs/alkaline etching	Textured surface/ /SiNWs/acidic etching	Textured surface/ /SiNWs/alkaline etching	Textured surface/SiNWs
Root mean square (r.m.s.), nm	599	813	624	771	1006	897
Maximum height of SiNWs, nm	3030	4026	3704	4151	5440	4137
Average height of SiNWs, nm	1786	1869	2180	2276	2328	1638
Degree of silicon porosity, %	82	99	98	92	96	56

acidic etchant resulted in an increase in sensor resistance from 42.5 to 79.4 Ω, while an alkaline etchant increased it from 42.5 to 54.1 Ω. This can be attributed to the significant increase in porosity from 56% to 96%, while the surface roughness remained almost unchanged, since the etching process primarily etched the surface layer with defects. Thus, the influence of these fabrication processes on resistance of the SiNWs array can be associated with an increase in bulk porosity and/or surface roughness, which likely disrupts the conducting channels and consequently leads to an increase in resistance.

The following process parameters contribute to a decrease in resistance of thermistors: increased etching time, increased amount of H_2O_2, and texturing of the surface. Increasing the duration of the second stage of MACE and presence of textured surface result in an increase in surface roughness and significant reduction of the surface porosity. This is expected to promote the formation of a greater number of conducting channels within the SiNWs array, thereby reducing the surface resistance of the sensors. Moreover, increasing the etching time leads to a change in the shape of the SiNWs array, which enhances the conductivity of the sensors (due to the connected together SiNWs by sidewalls). Changing t_2 from 45 to 135 min resulted in a decrease of resistance from 47.3 to 31.9 Ω. Texturing the sample surface before the MACE process reduced the sensor resistance from 106.4 to 54.1 Ω. It is worth noting that varying the hydrogen peroxide content from 0.4 to 1.2 ml resulted in a decrease in SiNWs resistance from 61.9 to 27.6 Ω, despite the increase in surface roughness and porosity. Clearly, treating the SiNWs in a concentrated hydrogen peroxide solution significantly affects the electrical characteristics of the sensors, which requires further investigation.

The thermosensitivity of resistive temperature sensors was determined as the relative change in resistance with temperature variation from 20 to 80°C. It was found that thermosensitivity exhibits a clear dependence on resistance, whereby an increase in sensor resistance leads to an increase in thermosensitivity (Table 2). Specifically, certain technological operations were identified to enhance thermosensitivity. Increasing the deposition time of silver nanoparticles from 20 to 60 sec. results in a significant increase in the coefficient of thermosensitivity from 221.1 to 985.4 ppm/K. Treatment with an alkaline etchant impairs an increase in thermosensitivity from 192.7 to 428.4 ppm/K, while, in the case of an acidic etchant, it increases from 192.7 to 785.8 ppm/K. This dependence of thermosensitivity on resistance is likely due to the increased degree of porosity, which provides a larger specific surface area involved in thermal generation of charge carriers.

A decrease in the resistance of the SiNWs array impairs deterioration in the thermosensitivity of resistive temperature sensors, attributed to a lower surface porosity and thermosensitive area of the sensor. Specifically, an increase in etching time and a presence of surface texturing result in a decrease in coefficient of thermosensitivity. For instance, increasing the etching time from 45 to 135 min leads to a decrease in the coefficient of thermosensitivity from 1628.3 to 812.3 ppm/K. The presence of surface texturing significantly reduces the coefficient of thermosensitivity to 192.7 ppm/K. Similarly, the change of H_2O_2 concentration from 0.4 to 1.2 ml results in a decrease of SiNWs thermosensitivity from 321.3 to 47.5 ppm/K. The influence of the two-step MACE etching process on thermosensitivity is likely due to electrical factors rather than structural factors (as surface roughness and porosity increase, along with the thermosensitive surface area). It could possibly have a negative impact on charge carrier lifetime. The maximum coefficient of thermosensitivity achieved for the resistive temperature sensor was 2335.8 ppm/K.

Temperature Diode Sensors. Thermodiodes operate based on the change in voltage drop across the p–n junction with temperature variation under constant current. The electrical and thermal sensitivity properties of diode-type temperature sensors based on SiNWs were investigated using voltage–current characteristics shown in Fig. 5, *a* and calculated rectification and thermosensitivity coefficients (Table 3).

Thermodiodes based on SiNWs are characterized by rectifying

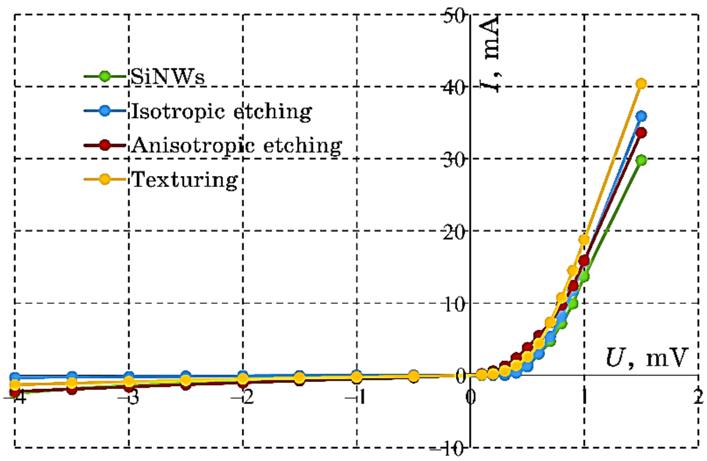

a

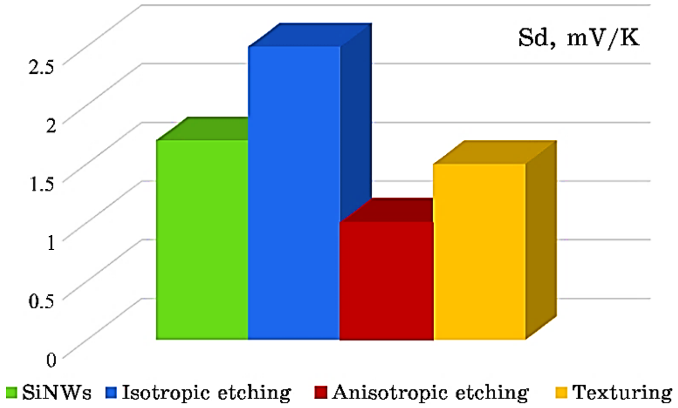

b

Fig. 5. *I*–*V* characteristics of thermodiodes based on SiNWs (*a*) and their thermosensitivity in dependence on additional chemical treatment (*b*).

properties, as confirmed by the *I*–*V* curves in Fig. 5, *a*. The rectification coefficients were calculated as the ratio of forward current to reverse one at a voltage of 1 V. In addition, the maximum rectification factor was 2503. The magnitude of thermosensitivity was determined using the equation

$$U(T) = U(T_0) - S\left(T - T_0\right),$$

where $U(T)$ and $U(T_0)$ are the applied biases at temperatures T and T_0 respectively, S is the thermosensitivity coefficient. Such a characteristic was measured at 100 μA current to avoid self-heating of the device, which would introduce errors in the measured temperature value.

TABLE 3. Electrical and thermosensitive parameters of resistive temperature sensors.

Sample number	1	2	3	4	5	6	7	8	100	102	105	109	110	111	113
R, Ω	61.9	27.6	38.1	47.3	31.9	65.7	91.8	54.4	199.6	67.3	106.4	85.3	54.1	79.4	42.5
S_r, ppm/K	321.3	221.1	47.5	1628.3	812.3	274.6	986.4	989.4	2335.8	1215.0	574.9	868.5	785.8	428.4	192.7

TABLE 4. Electrical and thermosensitive parameters of diode temperature sensors.

Sample number	1	2	3	4	5	6	7	8	100	101	102	104	105	109	110	111	112	113
K_{RR}	123	165	90	48	6	77	152	44	55	13	57	1924	2	2503	1745	32	54	90
S_d, мV/K	2.3	0.9	1.3	2	1.3	1.3	1.8	1.3	1.7	0.8	1.5	2.3	0.2	2	2.5	1	1.7	1.5

This research demonstrates that the process parameters of MACE significantly affect the rectification coefficient. The following technological parameters were found to improve rectifying characteristics. The variation in hydrogen peroxide content has shown that the best rectification coefficient was achieved at a concentration of 0.8 ml, resulting in a value of 165. This can be attributed to a non-monotonic increase in the forward current through the *p–n* junction.

However, further increase in the content of the second-stage reagent significantly deteriorates the electrical properties of the sensors. The presence of texture on the sensor surface improves rectification coefficient by 65%. This is due to an increase in the forward current through the *p–n* junction and a slight decrease in the reverse current. The use of additional etching by means of an isotropic etchant greatly improved the electrical characteristics of the diode sensors. In particular, the rectification coefficient increased by more than an order of magnitude (from 90 to 1745), which can be attributed to a one-order decrease in the reverse current through the *p–n* junction and a slight increase in the forward current.

It has also been found that increasing the duration of the first and second MACE stages has a negative effect on the electrical parameters of the sensors. Especially, changing of deposition time of Ag NPs from 20 to 60 sec reduces the rectification coefficient from 165 to 152, which can be explained by a two-fold decrease in the forward current through the *p–n* junction. In addition, changing of etching time in the range of 45 to 135 min decreases the rectification coefficient from 77 to 44. This is associated with an increase in the reverse current and a decrease in the forward current through the *p–n* junction. It has been shown that a higher content of $AgNO_3$ in the solution of the first stage leads to a decrease in the rectification coefficient from 165 to 55. This is due to a significant decrease in the forward current and an 80% increase in the reverse current through the *p–n* junction.

The use of additional etching by means of an anisotropic etchant resulted in an almost three-fold deterioration of the rectification coefficient, which is due to more than a two-fold increase in the reverse current through the *p–n* junction and a slight decrease in the forward current.

Increasing the duration of MACE first stage has an improving effect on the thermal sensitivity of the sensor, resulting in an increase of the thermal sensitivity coefficient from 0.9 to 1.8 mV/K. It is evident that increasing the surface roughness of the sensor from 226 to 753 nm provides an increase in the sensitive area of the sensor. However, when etching time is increased, temperature sensitivity of the device decreases by 35%. This observed trend may be attributed to the decrease in porosity, leading to a decrease in thermal sensitive area of the sensor. In addition, concentration of solution in the first stage of MACE ($AgNO_3$) improves of thermal sensitivity coefficient from 0.9 to 1.7 mV/K, which is due to an increase in the device's sensitive area. On the other hand, using a more concentrated solution at the second stage of MACE significantly decreases the sensor's sensitivity from 2.3 to 1.3 mV/K, despite an increase in surface roughness and porosity. It is evident that the positive effect of an increased sensitive area (roughness increased from 101 to 355 nm) is counteracted by the reduction in carrier lifetime during treatment in a concentrated hydrogen peroxide solution. Surface texturing reduces heat-sensitive characteristics more than twice. This deterioration in thermal sensitivity can be attributed to a sharp decrease in porosity of the silicon nanowire array from 82.5 to 56%. The use of additional etching on textured samples, using an acid etchant, improved the thermal sensitivity characteristics of the diode sensors from 1.5 to 2.5 mV/A. This improvement is attributed to the isotropic etching that smoothens the surface irregularities (reducing surface roughness from 897 to 771 nm), while significantly increasing the porosity (from 56 to 92%). However, when an alkaline etchant was used, the thermal sensitivity coefficient deteriorated by 50% despite the increased porosity coefficient which needs further explanation.

4. CONCLUSIONS

In this research, thermistors and thermodiodes based on silicon nanowires were developed, and the influence of MACE synthesis parameters on their characteristics was investigated.

It was determined that the technological synthesis parameters of the silicon nanowire array have a significant impact on lateral roughness and bulk porosity, which determine the specific surface area of the thermosensitive sensor surface and, consequently, affect the temperature sensitivity of the sensors.

Specifically, it was shown that increasing the parameters of the first stage of MACE and using acid etchant leads to an improved thermal sensitivity of both diode and resistive sensors. On the other hand, increase of the parameters of the second stage of MACE and the presence of surface texturing result in a deterioration of thermal sensitivity of both types of sensors. The maximum thermal sensitivity coefficients are as follows: 2336 ppm/K for thermoresistors and 2.5 mV/K for thermodiodes.

These results indicate that use of a simple and cost-effective nanowire synthesis technology (MACE) is efficient for production of resistive and diode temperature sensors.

REFERENCES

1. B. Sadoulet, D. Akerib, P. D. Barnes, A. Cummings, A. Da Silva, R. Diaz, J. Emes, S. Golwala, E. E. Haller, K. Itoh, W. Knowlton, F. Queinnec, R. R. Ross, D. Seitz, T. Shutt, G. Smith, W. Stockwell, and S. White, *Physica B: Condensed Matter*, **219**: 741 (1996); https://doi.org/10.1016/0921-4526(95)00871-3
2. Elder A de Vasconcelos, S. A Khan, W. Y Zhang, H. Uchida, and T. Katsube, *Sensors and Actuators A: Physical*, **83**: 167 (2000); https://doi.org/10.1016/S0924-4247(00)00351-4
3. Young-Jin Kim, Truong-Son Dinh Le, Han Ku Nam, Dongwook Yang, and Byunggi Kim, *CIRP Annals*, **70**, No. 1: 443 (2021); https://doi.org/10.1016/j.cirp.2021.04.031
4. Zahid Mehmood, Mohtashim Mansoor, Ibraheem Haneef, and S. Zeeshan Ali, *Sensors and Actuators A: Physical*, **283**: 159 (2018); https://doi.org/10.1016/j.sna.2018.09.062
5. Mohtashim Mansoor, Ibraheem Haneef, Suhail Akhtar, Andrea De Luca, and Florin Udrea, *Sensors and Actuators A: Physical*, **232**: 63 (2015); https://doi.org/10.1016/j.sna.2015.04.022
6. V. F. Mitin, V. V. Kholevchuk, R. V. Konakova, and N. S. Boltovet, *CAS '99 Proceedings of 1999 International Semiconductor Conference* (Cat. No. 99TH8389) (Sinaia, Romania: 1999), vol. **2**: pp. 495–498; doi:10.1109/SMICND.1999.810593
7. Natarajan Pradeep, Gopal Tamil Selvi, Uma Venkatraman, Quyet Van Le, Soon Kwan Jeong, Saravanan Pandiaraj, Abdullah Alodhayb, Muthumareeswaran Muthuramamoorthy, and Andrews Nirmala Grace, *Materials Today Chemistry*, **22**: 100576 (2021); https://doi.org/10.1016/j.mtchem.2021.100576
8. V. Koval, M. Dusheyko, A. Ivashchuk, S. Mamykin, A. Ievtushenko, V. Barbash, M. Koliada, V. Lapshuda, and Roman Filov, *Proc. of Symp. '2020 IEEE 40st International Conference on Electronics and Nanotechnology (ELNANO)' (22–24 April, 2020)* (Kyiv: Igor Sikorsky Kyiv Polytechnic Institute: 2020), p. 246; https://doi.org/10.1109/ELNANO50318.2020.9088736
9. Mrinmoy Kumar Chini, Vishal Kumar, Ariba Javed, and Soumitra Satapathi, *Nano-Structures & Nano-Objects*, **19**: 100347 (2019); https://doi.org/10.1016/j.nanoso.2019.100347
10. V. Koval, Yu. Yakymenko, A. Ivashchuk, M. Dusheyko, M. Fadieiev, T. Borodinova, and D. Didichenko, *Proc. of Symp. '2018 IEEE 38st International Conference on Electronics and Nanotechnology (ELNANO)' (24–26 April, 2018)* (Kyiv: Igor Sikorsky Kyiv Polytechnic Institute: 2018), p. 186–190; https://doi.org/10.1109/ELNANO.2018.8477552
11. V. Lapshuda, V. Koval, V. Barbash, M. Dusheiko, O. Yashchenko, and S. Malyuta, *Proc. of Symp. '2022 IEEE 41st International Conference on Electronics and Nanotechnology (ELNANO)' (Oct. 10–14, 2022)* (Kyiv: Igor Sikorsky Kyiv Polytechnic Institute: 2022), p. 208; https://doi.org/10.1109/ELNANO54667.2022.9927092
12. Yi Xin, Junye Tong, Tianyuan Hou, Hongyan Liu, Meng Cui, Xuefeng Song, Yuhang Wang, Tingting Lin, Lingling Wang, and Gang Wang, *Measurement.*, **212**: 112694 (2023); https://doi.org/10.1016/j.measurement.2023.112694
13. V. M. Koval, A. V. Ivashchuk, Yu. I. Yakymenko, M. G. Dusheyko,

Yu. V. Yasievich, G. S. Khrypunov, and E. I. Sokol, *Radioelectronics and Communications System*, **59**, No. 2: 53 (2016); http://dx.doi.org/10.3103%2FS0735272716020011
14. V. Abhikha Sherlin, Megha Maria Stanley, Sea-Fue Wang, Balasubramanian Sriram, Jeena N. Baby, and Mary George, *Food Chemistry*, **423**: 136268 (2023).
15. M. G. Dusheiko, V. M. Koval, and T. Yu. Obukhova, *Quantum Electronics & Optoelectronics*, **25**, No. 1: 058 (2022); https://doi.org/10.15407/spqeo25.01.058
16. Nagaraj P. Shetti, Amit Mishra, Soumen Basu, and Tejraj M. Aminabhavi, *Materials Today Chemistry*, **20**: 100454 (2021); https://doi.org/10.1016/j.mtchem.2021.100454
17. A. Orlov, V. Ulianova, A. Zazerin, O. Bogdan, G. Pashkevich, and Y. Yakymenko, *Radioelectronics and Communications Systems*, **59**, No. 2: 60 (2016); https://doi.org/10.3103/S0735272716020023
18. Nagy L. Torad, Islam M. Minisy, Hadir M. Sharaf, Jaroslav Stejskal, Yusuke Yamauchi, and Mohamad M. Ayad, *Synthetic Metals*, **282**: 116935 (2021); https://doi.org/10.1016/j.synthmet.2021.116935
19. Gengfeng Zheng, *Semiconducting Silicon Nanowires for Biomedical Applications* (Ed. Jeffery Coffer). *Ch. 2. Growth and Characterization of Silicon Nanowires for Biomedical Applications* (Woodhead Publishing: 2022); https://doi.org/10.1016/B978-0-12-821351-3.00002-1
20. Madhu Sudan Saha, Ruying Li, and Xueliang Sun, *Journal of Physics and Chemistry of Solids*, **156**: 110146 (2021); https://doi.org/10.1016/j.jpowsour.2007.11.036
21. V. Koval, Yu. Yakymenko, A. Ivashchuk, M. Dusheyko, O. Masalskyi, M. Koliada, and D. Kulish, *Proc. of Symp.* '*2019 IEEE 39st International Conference on Electronics and Nanotechnology (ELNANO)*' *(16–18 April, 2019)* (Kyiv: Igor Sikorsky Kyiv Polytechnic Institute: 2019), p. 282–287; https://doi.org/10.1109/ELNANO.2019.8783506
22. Amit Solanki and Handon Um, *Semiconductors and Semimetals*, **98**: 71 (2018); https://doi.org/10.1016/bs.semsem.2018.04.001
23. Peng Yu, Jiang Wu, Shenting Liu, Jie Xiong, Chennupati Jagadish, and Zhiming M. Wang, *Nano Today*, **11**: 704 (2016); https://doi.org/10.1016/j.nantod.2016.10.001
24. Nafis Ahmed, P. Balaji Bhargav, Arokiyadoss Rayerfrancis, Balaji Chandra, and P. Ramasamy, *Materials Letters*, **219**: 127 (2018); https://doi.org/10.1016/j.matlet.2018.02.086
25. Bagur R. Deepu, Seegehalli M. Anil, Purakkat Savitha, and Yeriyur B. Basavaraju, *Vacuum*, **185**: 109991 (2021); https://doi.org/10.1016/j.vacuum.2020.109991
26. A. Fasoli and W. I. Milne, *Materials Science in Semiconductor Processing*, **15**: 601 (2012); https://doi.org/10.1016/j.mssp.2012.05.010
27. Yaroslav Linevych, Viktoriia Koval, Mykhailo Dusheiko, Yuriy Yakymenko, Maryna Lakyda, and Valerii Barbash, *Proc. of Symp.* '*2022 IEEE 41st International Conference on Electronics and Nanotechnology (ELNANO)*' *(Oct. 10–14, 2022)* (Kyiv: Igor Sikorsky Kyiv Polytechnic Institute: 2022), pp. 190–195; https://doi.org/10.1109/ELNANO54667.2022.9927122